Ni-Alumina Dry Reforming Catalysts: Atomic Layer Deposition and the Issue of Ni Aluminate

Patrick Littlewood[1], Shengsi Liu[1], Eric Weitz[1], Tobin J. Marks[1], Peter C. Stair[1]
1 Department of Chemistry, Northwestern University, Evanston, Illinois 60208 (USA)

Abstract

A catalyst consisting of 2 wt% Ni supported on a commercially available transition alumina is modified using TMA-H_2O ALD cycles to deposit thin alumina overcoats on the catalyst, and it is then investigated for the catalytic dry reforming of methane (DRM) at 700 °C. Highly dispersed Ni rapidly sinters to form bulk Ni particles on the uncoated catalyst. In contrast, deposition of an alumina overcoat by ALD significantly lowers the rate of Ni sintering, and also lowers the propensity towards carbon deposition during DRM. Additionally, it is experimentally demonstrated that the Ni aluminate ($NiAl_2O_4$) spinel phase is unstable under the present DRM conditions and slowly undergoes reduction to metallic Ni and Al_2O_3. Slow reduction of the Ni^{2+} from $NiAl_2O_4$ is proposed as the origin of the large increase in DRM activity observed for the alumina-overcoated Ni catalysts.

1. Introduction

The dry reforming of methane (DRM) reaction can be used for the highly desirable transformation of two abundant low-value gases into an industrially useful feedstock (eq. 1). [1] The high

$$CH_4 + CO_2 \rightleftharpoons 2\ CO + 2\ H_2 \quad (1)$$

endothermicity of this reaction (+247 kJ mol^{-1}) makes it thermodynamically unfavorable and consequently, high temperatures (upwards of 600-700 °C) must be employed to obtain appreciable conversions in a standard reactor. The stoichiometry of DRM affords a maximum H_2 : CO ratio of 1 when reverse water gas shift (RWGS) is the only side reaction, since RWGS reduces the H_2 yield per pass (eq. 2). Additionally,

$$H_2 + CO_2 \rightleftharpoons CO + H_2O \quad (2)$$

slow carbon-forming side reactions can also occur and cause catalyst deactivation (eqs. 3, 4). Carbon can encapsulate the active site and render it inaccessible to the gas feed.[2][3] However, carbon

$$CH_4 \rightleftharpoons C + 2\ H_2 \quad (3)$$

$$2\ CO \rightleftharpoons C + CO_2 \quad (4)$$

deposition does not necessarily deactivate the catalyst. For example, carbon nanotubes can form underneath the active particle and push it away from the support surface without severely compromising the catalytic activity.[2][3] Another major mechanism for deactivation is particle sintering, typically via particle coalescence and/or Ostwald ripening.[4] It has been shown that larger Ni particles are more favorable for coking due to ensemble size effects, with the ensemble size being a measure of the number of active sites in close mutual proximity.[5] This means that sintering can subsequently increase the rate of carbon deposition. Mechanisms of deactivation are therefore often interdependent and challenging to disentangle in terms of mechanistic elucidation.

The stabilities of Ni-based catalysts are, in general, lower than those of their Pt, Pd, etc. counterparts, owing largely to higher rates of carbon deposition, in particular for DRM, where the carbon content of the feed is high.[6] However, supported Ni catalysts are used extensively at high temperatures to reform natural gas, because of their high activity and lower cost than noble metal catalysts.[5]

Overcoating with an oxide by atomic layer deposition (ALD) has been used as a design strategy to enhance the performance of heterogeneous metallic catalysts.[7] Increases in catalytic activity and/or stability have been achieved by creating overcoats using titania ALD[8] and zirconia ALD,[9] and by using wet methods to generate silica overcoats.[10][11] In particular, catalysts with alumina ALD overcoats have shown increased resistance to both sintering and coking.[12][13] Gould *et al.* dramatically enhanced the stability of Ni DRM catalysts by depositing alumina around a molecular template to produce a structured microporous extension of the support.[14] However, a thorough understanding of the behavior and effect on catalytic activity and selectivity of such an ALD alumina overcoat under harsh DRM reaction conditions has yet to be achieved.

Phase change is one of the many phenomena known to affect the activity of heterogeneous catalysts. However, it is sometimes overlooked due to the mismatch between the very short timescales typically involved in creating a kinetically stable solid-state material (for a given temperature) and the very long timescales involved in achieving thermodynamic stability. For example, transition aluminas are metastable intermediates in the formation of the thermodynamically stable α-Al_2O_3 phase, but make excellent, thermally and chemically stable catalyst supports under most practical operating conditions.[15] Similarly, the $NiAl_2O_4$ phase has been observed both before, during, and after DRM catalysis, variously described as having an inert, deactivating, or stabilizing effect on the catalyst, as described in the following examples. The formation of Ni aluminate and the subsequent high temperature reduction by H_2 from Ni^{2+} to the active Ni^0 has been previously shown to yield smaller Ni crystallites than formed from the reduction of bulk NiO.[16,17] Recently, the migration of Ni into an alumina support under dry reforming conditions to form $NiAl_2O_4$, which deactivates the catalyst, was reported.[18] In contrast, calculations by Deutschmann and co-workers predict that spontaneous oxidation of Ni by water or CO_2 to $NiAl_2O_4$ should not occur under reforming conditions due to positive Gibbs reaction energies.[19] The studies referenced show that although Ni aluminate is not considered to be catalytically active for dry reforming, its presence can be profound because of its effect on the active site for catalysis, although it is not clear how. In this contribution we use alumina ALD and high temperature annealing to explore the effects of an overcoat and phase change on a typical Ni DRM catalyst.

2. Methods and Experimental

Preparation of Ni/Al_2O_3: The supported Ni catalyst was prepared by incipient wetness impregnation of commercial CATALOX SBa-90 Sasol Al_2O_3 (5.0 g) with $Ni(NO_3)_2 \bullet 6H_2O$ (505 mg) in 5 mL acetone. The powder was dried overnight before calcination in air at 550 °C for 2 h with a ramp rate of 5 °C/min. For one sample, specifically noted in the text, the calcination temperature was not 550 °C but 700 °C. All samples were reduced in-situ at 500 °C in 30 mL min^{-1} 10% H_2 in N_2 immediately before catalytic testing.

ALD overcoatings were performed on the unreduced, calcined samples in an Arradiance Gemstar ALD reactor operating at 125 °C using trimethylaluminium (TMA) and water, with N_2 as the purge gas. Materials with 5 and 20 ALD cycles were prepared using previously described procedures.[12] Timing sequences for the ALD cycles are expressed in the form t_1-t_2-t_3-t_4, where t_1 is the dose and hold duration (in sec) of the "A" precursor (TMA), t_2 is the duration of the corresponding purge, t_3 is the duration of the "B" precursor dose and hold time (H_2O), and t_4 is the duration of its corresponding purge. All times are in seconds. For TMA/H_2O, approximately 200 mg of substrate was loaded into the reactor and a timing sequence of 6-60-6-60 was used, with t_1 and t_3 each corresponding to a 1 s vapor pulse and a 5 s stagnant "soak" with no reactor flow. Longer dose, hold, and purge times were also investigated and gave no additional deposition. It should be noted that these dose/purge times may be reactor specific.

Catalytic evaluations were carried out in the CleanCat facility of Northwestern University using mass flow controllers and a "clam-type" furnace with a thermocouple located directly in the catalyst bed (Altamira Instruments). Gas analysis was performed using an Agilent 6850 GC with 0.32 mm CarbonPlot column and TCD detector. Gases were provided by Airgas and were used without further purification. The catalyst was mixed with 1 ml quartz sand and loaded onto a bed of quartz wool in a tubular quartz reactor (internal diameter of 8 mm). BET N_2 physisorption surface areas were measured in the CleanCat facility using a Micromeritics 3-Flex instrument. BJH pore volumes were calculated based on desorption curves. Powder X-Ray Diffraction (PXRD) was performed at the JB Cohen facility of Northwestern University using a Scintag XDS2000 with a CuKα source and solid state detector, using slits of 4.0, 2.0, 1.0, and 0.75 mm (source to detector). UV-Visible diffuse reflectance spectroscopy (UV-Vis-DRS) was carried out using a Shimadzu UV-3600 spectrophotometer equipped with a Harrick Praying Mantis diffuse reflectance accessory.

3. Results and Discussion

BET surface areas of the materials employed in this study are shown in Table 1. The surface area and pore structure of the catalyst support remain unchanged even after exposure to aggressive sintering conditions (3 days at 700 °C under a mixed flow of N_2 and water vapor). Impregnation with 2 wt% Ni also did not affect the porosity or surface area, even after reduction.

Overcoating of the catalyst with 20 ALD cycles resulted in a dramatic decrease in surface area, attributed to filling and blocking of the pores within the support. However, upon reducing the catalyst for 1 h at 500 °C in flowing H_2, much of the surface area and some of the pore volume is recovered. Comparing the pore size distributions from BJH calculations, the uncoated and freshly overcoated catalysts both have a single peak at 150 Å indicating that the overcoat conforms to the pore morphology of the support (Figure 1). The major peak for the overcoated catalyst is shifted to a slightly lower pore diameter due to lining of the pore walls and is lower in magnitude in accordance with the lower surface area. However, the reduced overcoated material has additional peaks below this major 150 Å feature. High temperature reduction is known to create new pores or fissures within the overcoat itself.[13] BET and BJH data are summarized in Table 1.

Table 1. BET surface areas and BJH pore volumes determined by N_2 physisorption

Sample	BET Surface Area, $m^2 g^{-1}$	BJH Pore Volume, $cm^3 g^{-1}$
Al_2O_3 support (fresh)	101	0.41
Al_2O_3 support (3 days 700 °C + steam)	107	0.43
Ni/Al_2O_3 (fresh)	101	0.40
Ni/Al_2O_3 (reduced)	105	0.41
Ni/Al_2O_3 (after 20 h DRM at 700 °C)	99	0.42
Overcoated sample (fresh)	53	0.17
Overcoated sample (post reduction)	82	0.24

Figure 1. BJH desorption pore size distributions of catalysts before and after thermal treatment.

X-ray diffraction (XRD) patterns of the fresh support exhibit major features for θ-alumina (PDF 98-000-0060) with a minority γ-alumina (PDF 98-000-0059) phase (Figure 2).[15] These reflections remain unchanged and no α-alumina (PDF 01-082-1467) phase is detectable after thermal treatment at 700 °C. After Ni impregnation and calcination at 550 °C or 700 °C, no features attributable to Ni-related crystallites have been observed, indicating that high Ni dispersion is preserved.

Figure 2. Power x-ray diffraction (PXRD) patterns of the alumina support (”fresh support”), the support after 3 days in N_2 and water vapor at 700 °C (“Al_2O_3 3 days 700 °C + H_2O”), and overnight in air at 700 °C (“Al_2O_3 overnight 700 °C”), and after IW impregnation with $Ni(NO_3)_2$ and subsequent calcination at 550 °C (“2% Ni/Al_2O_3 550 °C”) or 700 °C (“2% Ni/Al_2O_3 700 °C”). Standard peak positions are indicated by vertical blue lines for γ-alumina (PDF 98-000-0059), red lines for θ-alumina (PDF 98-000-0060) and green lines for NiO (PDF 00-001-1239).

Recent publications involving dispersed alumina supported Ni catalysts have highlighted the question of Ni migration into the alumina framework as a mechanism of catalyst deactivation, [18] as previously shown for Co supported on alumina at low loadings.[20] In contrast, it was recently shown that, unlike $CoAl_2O_4$, Ni aluminate ($NiAl_2O_4$) should not be formed from reduced, alumina-supported Ni under DRM conditions due to the positive Gibbs reaction energy.[19] Due to the difficulty in distinguishing Ni phases at low loadings and high dispersions by XRD, $NiAl_2O_4$ was prepared in the current investigation by calcining the uncoated supported Ni catalyst in air at 1100 °C. Under these conditions, the bulk transition alumina becomes α-alumina ((PDF 01-082-1467) and highly crystalline $NiAl_2O_4$ (PDF 01-071-0964) is formed from reaction with the NiO, as shown in the XRD pattern in Figure 3.

Figure 3. PXRD of fresh alumina support as-received, alumina support after high temperature calcination, and after Ni impregnation and subsequent high temperature calcination.

Existing literature highlights the effect of the different coordination environments of Ni^{2+} cations on the absorbance of visible, UV and near IR light.[21][22][23] Unreduced materials were characterized by UV-Vis-DRS, shown in Figure 4, using the CATALOX alumina support as a reference for the

Kubelka-Munk transform. The lower section of Figure 4 shows the UV-Vis-DRS spectra of the as-prepared materials calcined at 550 °C, calcined at 700 °C, and calcined at 550 °C before applying an ALD overcoat of 20 cycles of alumina, and the upper section of Figure 4 shows the as-prepared (uncoated) material after calcination in air at 1100 °C (see Figure 6). Bands at 715 nm and 377 nm (labelled α in Figure 4) are caused by the octahedrally coordinated Ni^{2+} species in the NiO lattice, whereas absorption in the range of 600–645 nm (labelled γ in Figure 4) results from tetrahedrally coordinated Ni^{2+} in the $NiAl_2O_4$ lattice.[21] Absorption at around 410 nm (labelled as β in Figure 4) has been previously attributed to Ni^{2+} in a distorted octahedral coordination, such as in $NiAl_2O_4$.[24,25] Note that the strong absorption from the reference alumina support disproportionately affects the data below 350 nm and peaks in this region were therefore not compared between different UV-Vis-DRS experiments. Although there are inherent challenges in the quantitative comparison of diffuse reflectance data between separate experiments, the relative magnitudes of the γ bands in comparison to the α bands (in particular the band at 377 nm) indicate the relative populations of surface Ni^{2+} cations tetrahedrally coordinated as $NiAl_2O_4$ in comparison to NiO. However, it should be noted that the oscillator strengths of d-d transitions of tetrahedrally coordinated Ni^{2+} are higher than those of octahedrally coordinated Ni^{2+} due to the selection rules.[24][26] The material calcined at 550 °C exhibits high absorbance in the NiO region(s) with relatively little indication of the presence of $NiAl_2O_4$. In contrast, the material calcined at 700 °C shows absorbances similar to the material calcined at 1100 °C for which the bulk Ni^{2+} can be considered to be mostly in the $NiAl_2O_4$ phase (see Figure 3). It is known that calcination of alumina supported Ni catalysts at high temperatures causes Ni^{2+} to form $NiAl_2O_4$,[27] and this clearly occurs to a significantly greater extent at 700 °C than at 550 °C. After reduction in H_2 and transfer to the UV-Vis-DRS cell, the materials exhibit broad and intense absorption bands, presumably caused by the presence of metallic Ni, which obscures the features labelled in Figure 4, and the UV-Vis-DRS data for these materials are therefore uninformative.

Comparison of the UV-Vis spectra for the uncoated materials with the spectrum observed for the overcoated material (with no further treatment after ALD) presents a greater challenge in interpretation. The total absorbance from Ni^{2+} related bands is lower than for the uncoated materials, and the relative intensities of the $NiAl_2O_4$ bands to the NiO bands are higher than for the material calcined at 550 °C but lower than for the $NiAl_2O_4$ material or the material calcined at 700 °C. The most likely interpretation concerns the changing symmetry of Ni^{2+} at the surfaces of NiO. The absorption seen at position α is attributed to d-d transitions, which, as noted above, are formally Laporte forbidden in regular octahedra such as the coordination environment of NiO in the fcc lattice. Relaxation of this selection rule occurs mainly as a result of distortions in the geometry, static or otherwise.[26] Interactions with Al^{3+} in the ALD layer should affect the geometries of such terminal, octahedrally coordinated Ni^{2+} and thus alter the oscillator strengths of d-d transitions. Because the NiO is highly disperse (Figure 2), it is possible that the ALD layer affects the already distorted symmetry of a large portion of the absorbing octahedral Ni^{2+} species, significantly altering the intensities of the various bands seen in Figure 4 with little or no change in the concentration of octahedrally coordinated Ni^{2+} in the sample. Alternatively, an unlikely interpretation is that some of the NiO forms $NiAl_2O_4$ during ALD, and difficulties in obtaining quantitatively reproducible diffuse reflectance from a powder surface result in a lower overall absorbance. This is unlikely because the temperatures used for ALD are very mild compared to those required to form the spinel phase, both as reported in the literature and as seen in the present work (note that this does not exclude the

possibility that $NiAl_2O_4$ forms in this material when it is heated to higher temperatures). Reduction of the octahedral Ni^{2+} to a Ni^0 species, for example by reaction with TMA, would also cause a decrease in intensity for the octahedral peaks labelled as α. However, the broad intense absorption which dominates the spectra of all samples reduced in H_2 cannot be seen in Figure 4, implying that metallic Ni is not present. With a lack of evidence for other Ni-containing species, it is therefore problematic to consider the spectrum as indicative of a loss of NiO.

Figure 4: UV-Vis-DRS spectra for various materials, using the CATALOX alumina support as a reference. Top: spectra of $NiAl_2O_4$-based material prepared by calcining the uncoated catalyst at 1100 °C in air. Bottom: spectra of uncoated 2 wt% Ni/Al_2O_3 after calcination in air at 700 °C, 550 °C, and 550 °C followed by 20 cycles of alumina ALD. Vertical lines indicate expected positions of absorbance bands for octahedrally (α and β) and tetrahedrally (γ) coordinated Ni^{2+}.

All catalysts were investigated for activity in the DRM reaction (Figure 5). The fresh uncoated catalyst exhibits impressive activity at the beginning of the reaction period owing to the high dispersion of the Ni species on the support surface.[28] However, rapid and supralinear deactivation occurs leading to a ten-fold decrease in activity after ca. 15 h time on stream. Focusing on the characteristic Ni diffraction region in the XRD, in Figure 6 it can be seen that after reduction the uncoated catalyst has no visible metallic Ni (or NiO) features (expected at 2θ = 51.7 for Ni, PDF 03-065-0380), consistent with small and highly dispersed Ni domains. However, after reaction, Ni crystallites are clearly observable by XRD. Note that the catalytic activity is not regenerable by oxidation at 700 °C and re-reduction to remove carbon deposits (shown in the SI). The major mechanism of deactivation for the uncoated catalyst is therefore consistent with Ni particle sintering.

Figure 5. Activity of Ni/Al_2O_3 catalysts calcined at 550 °C with and without an alumina (TMA-H_2O) ALD overcoat, and calcined at 700 °C without an overcoat. The same data are shown (inset) after having been normalized to the fraction of the maximum activity for each sample, to highlight catalyst stability. T = 700 °C, GHSV = 360 L h^{-1} g_{cat}^{-1} (overcoated), 1350 L h^{-1} g_{cat}^{-1} (700 °C), 3600 L h^{-1} g_{cat}^{-1} (550 °C), CH_4:CO_2:He = 1:1:8. The initial data shown within the first 3 hours were obtained at reaction temperatures of 500 °C and 600 °C, while ramping up to 700 °C.

The material calcined at 700 °C exhibits a gradual increase in activity over a period of 10-15 h. Note that this activity increase is not caused by the temperature ramp up to 700 °C, which is complete within the first 3 h. The period of increasing activity is followed by slow linear deactivation of approx. 60% over the next 25 h.

Note that ALD overcoating of the catalyst results in a significantly lower initial DRM activity, presumably due to encapsulation of most of the initial Ni active sites by the ALD alumina. However, the stability of the catalyst is also substantially improved. To highlight the effect of overcoating on stability, the inset to Figure 3 shows the activity normalized to a maximum of unity for each data set. Increasing numbers of ALD cycles afford decreasing initial activity and increasing stability. After 20 ALD cycles, the catalytic activity initially increases over a period of *ca.* 20 h, in a similar way to the uncoated material calcined at 700 °C. Also similar to the catalyst calcined at high temperature, the

activity increase is followed by slow deactivation, but at a lower rate (than for the uncoated material) of *ca.* 25% over the next 40 h.

5 cycles of alumina deposition results in a slight increase in stability with a lower rate of deactivation. Thus, this catalyst effectively exhibits a combination of the behaviors of the uncoated material and the material after 20 ALD cycles. This is in marked contrast to a core-shell material prepared from bulk NiO nanoparticles, for which 5 alumina ALD cycles gives the same stability as 20 cycles, but with higher catalytic activity.[12] The effect of the number of TMA-H_2O ALD cycles on DRM catalysis is therefore specific to the starting catalytic material used. Because of its lower performance, the material with 5 ALD cycles was not investigated further and through the rest of this study the material with 20 ALD cycles will be simply referred to as "overcoated".

Due to the different activities of the materials tested, and the very different rates of deactivation, comparison of the materials at the same conversions for extended periods of time was not possible with the fixed-flow apparatus used. To account for the very different activities, the masses of each catalyst were chosen so that all tests were performed at measurable conversions away from the thermodynamic equilibrium.

Figure 6. XRD patterns of the catalyst support before impregnation with Ni, and the Ni catalyst after H_2 reduction, after 20 h DRM reaction, and after overcoating and 20 h DRM. Note the presence of Ni^0 crystallites after 20 h DRM reaction and the absence of them for the bare support and the reduced catalyst.

Alumina deposited by ALD is initially amorphous and highly hydroxylated, requiring thermal treatment to restructure.[29] In order to separate thermal effects from the effects of the DRM or H_2 reduction environments, various high temperature pre-treatment conditions were investigated before DRM. All pre-treatments were performed at 700 °C, which is the maximum temperature used for reaction in this study. As shown in Figure 7, the initial behavior of the overcoated catalyst is affected by changing the atmosphere and by changing the time duration of the pre-treatment conditions used. Treating the catalyst for 12 h in a flow of He results in an increase of initial activity, which is smaller than the activity increase induced by treating the catalyst for the same length of time in a reducing environment (10 % H_2 in N_2). Note also that the maximum activity in each case is different. Both the initial and the maximum activities of catalysts are higher with more aggressive pre-treatment. This result indicates that a mixture of activating and deactivating processes are occurring under the different conditions. In particular, a major pathway of deactivation only occurs (or occurs rapidly) under dry reforming conditions. The literature suggests that this is likely due to carbon deposition, and/or higher rates of Ni sintering caused by the presence of water.[5]

It has been shown that the amorphous alumina films deposited by ALD on alumina substrates rapidly and irreversibly form pores above *ca.* 500 °C.[30] The BET data demonstrate that this also occurs for the catalyst discussed here. An increase in porosity could reasonably lead to an increase in activity by exposure of previously inaccessible active sites. However, comparison of the timescales for pore formation reported in the literature [30][31], and the activity increase observed here, indicate that this is probably not the principal origin of the change in initial activity (which is different after isothermal treatments of 12 h and 72 h) or the slow and gradual increase in activity seen in Figure 7

(which occurs over around 20 h). However, the aforementioned study by Karwal *et al.* did not investigate timescales of tens of hours. Moreover, continual growth of pores by slow sintering is a well-known phenomenon for ceramic materials.[32] The effect of changing the gas phase from He to 10% H_2 in N_2 would also be difficult to account for if the principal cause of the activity increase were the thermal formation of porosity in the ALD film.

Figure 7. Activity of alumina overcoated Ni/Al_2O_3 DRM catalysts after various pre-treatment conditions. Conversion is shown as a dimensionless fraction (0.00-1.00). All pre-treatment performed at 700 °C. Reaction T = 700 °C, GHSV = 360 L h^{-1} g_{cat}^{-1}, CH_4:CO_2:He = 1:1:8.

The $NiAl_2O_4$ material (after calcination at 1100 °C) was evaluated for the DRM reaction at 700 °C. $NiAl_2O_4$ is not an active DRM catalyst,[33] but the activity gradually increased with time on stream (Figure 8) in concert with disappearance of the spinel phase as evidenced by the PXRD patterns shown in Figure 9. We therefore conclude that $NiAl_2O_4$ is not a stable phase under the DRM conditions used for this experiment. Consequently, formation of Ni aluminate cannot be the cause of significant catalyst deactivation in this study. Instead, reduction of Ni^{2+} in the inactive $NiAl_2O_4$ phase to metallic Ni, which is the catalytically active form of Ni for DRM, is not only thermodynamically favored under the conditions used, but must occur for the catalyst to show any activity at all. The unfavorable kinetics in reducing $NiAl_2O_4$ even at high temperatures is the most likely reason for the slow increase in activity seen in Figure 8. The pronounced similarity in catalytic behavior (Figure 5 and Figure 8) and optical absorption properties (Figure 4) between the two uncoated catalysts calcined at 700 °C and 1100 °C, along with the contrasting catalytic and light absorption properties of the uncoated catalyst calcined at 550 °C, are consistent with this description of slow $NiAl_2O_4$ reduction as the cause of the lengthy period of increasing activity. This explanation is also consistent with previous studies on bulk $NiAl_2O_4$ or high loading NiO/Al_2O_3 under methane reforming conditions,[33][34] but different from that observed recently by Coperet and co-workers for a catalyst with lower Ni loading at lower temperatures. Whether the direction of the NiO to $NiAl_2O_4$ reaction is a function of catalyst preparation or reaction conditions, it is arguable that the phases in the as-prepared materials both here and in similar work elsewhere,[35][36] are far from thermodynamic equilibrium, as evidenced by the presence of transition alumina, and therefore the phase transformations are in all likelihood kinetically controlled.

The similarity between the catalytic behaviors of the $NiAl_2O_4$ containing materials and the overcoated catalyst in the first ~20 h are informative. It is likely that after heating to reaction temperature the overcoated catalyst also contains a significant quantity of $NiAl_2O_4$, which must slowly reduce under reaction conditions before the maximum activity is reached. This $NiAl_2O_4$ could form when the amorphous alumina overcoat initially restructures over dispersed, as-synthesized NiO at elevated temperatures, despite the presence of H_2 in the gas phase. This description agrees with the results shown in Figure 7, which demonstrate an increase in catalyst activity after prolonged exposure to H_2. It also implies that $NiAl_2O_4$ will slowly undergo reduction at 700 °C in an inert gas, as is known to occur rapidly under O_2-free conditions at higher temperatures.[37]

Figure 8. DRM activity of $NiAl_2O_4$. T = 700 °C, GHSV = 360 L h^{-1} g_{cat}^{-1}, CH_4:CO_2:He = 1:1:8. The y-axis is fractional conversion (0.0 - 1.0).

Note that Gould *et al.* reported a very similar slow increase in DRM catalytic activity for supported Ni catalysts overcoated with a microporous alumina framework deposited by molecular layer deposition (MLD) using TMA, water, and a sacrificial organic template molecule.[14] They reported that the activity increase was consistent with "both reduction of NiO under the MLD film and pore expansion within the MLD film so as to uncover more metal surface area," although all the evidence they present points towards reduction of oxidized Ni as the principal cause (see also the Supporting Information for [14]). The agreement of their results with those presented here implies that calcination indeed causes severe loss of active sites through Ni oxidation to a species which is far more difficult to reduce, and which could not be reduced in H_2 at 500 °C before DRM. We hypothesize that the NiO could have reacted with the deposited alumina to form $NiAl_2O_4$ upon calcination and structural reorganization of the amorphous alumina overcoat, and that this new phase cannot be clearly detected by XRD alone, presumably due to small crystallite size or density.

In the aforementioned study, the Ni oxidation state before MLD appears to be zero. The material presented in the current work was calcined in air at 550 °C before overcoating. Both materials initially have low catalytic activities for DRM, which dramatically increase over approximately 20 h at 700 °C. Considering the similarities between the catalytic behaviors of the two materials, the oxidation state of Ni at the point of deposition appears to have little effect on the ultimate behavior of the catalyst during DRM.

Figure 9. Enlarged PXRD of a 2% Ni/Al_2O_3 DRM catalyst after high temperature oxidation to convert all Ni to $NiAl_2O_4$ and extended DRM at 700 °C (see Figure 7). Vertical dashed lines indicate peak positions for the spinel $NiAl_2O_4$ (PDF 01-071-0964) phase (full PXRD in SI).

When Gould *et al.* used a lower calcination temperature of 400 °C after MLD, a much higher starting activity per gram of Ni was observed and the activity consistently decreased with time on stream. This is in stark contrast to the behavior of both the same material calcined at 500 °C after MLD, and the present catalyst which was not calcined after ALD. It is probable that the temperature of overcoat structural rearrangement is around 500 °C.[30] If the amorphous alumina overcoat indeed reacts with Ni to form $NiAl_2O_4$ when the temperature is ramped up, it is likely that Ni^{2+} is more reactive than Ni metal and thus forms $NiAl_2O_4$ more readily. We therefore suggest that the catalytic activity and stability are related to formation and reduction of $NiAl_2O_4$, the extent of which is determined by the oxidation state of Ni at the point at which the overcoat undergoes structural changes from thermal treatment.

Table 3 shows the amount of carbon deposited in two separate experiments designed to maintain similar conversions for both catalysts of around 0.2-0.4 (see SI). The overcoated sample generates significantly less carbon per gram of catalyst. Less carbon was also generated per mole of CH_4 reacted, indicating that the active sites of the overcoated catalyst are inherently less selective towards carbon deposition. Note that the overcoated catalyst is more resistant to carbon

Table 3. Amount of carbon deposited over 20 h tests of each DRM catalyst. The mass of catalyst (2 mg for uncoated sample, 20 mg for overcoated) was altered to maintain similar conversions (0.2-0.4) between tests and thus similar chemical potentials for carbon deposition.

	Total Carbon Deposited		
	μmols	**μmols g_{cat}^{-1}**	**μmols mol_{CH4}^{-1}**
Uncoated	3.9	1.95	13.3
Overcoated	2.6	0.13	4.9

deposition under the conditions used. The increased resistance of Ni to sintering after an overcoat is deposited could accordingly affect carbon deposition simply by maintaining a small Ni particle size.[38][39] There is also evidence that greater metal-support interactions can lead to lower rates of carbon deposition. Using $NiAl_2O_4/Al_2O_3$ as a catalyst precursor phase was shown to result in lower rates of catalyst coking than NiO/Al_2O_3 due to claimed "stronger metal-support interactions" although no direct evidence thereof was provided.[40] It is also possible that the lower rates of carbon deposition on the overcoated catalyst are attributable to interactions of the alumina overcoat with the Ni sites. This has been attributed in the literature to reaction at the Ni-alumina interface and/or to extended electronic effects.[41] More specifically, on the one hand, this could be caused by selective poisoning or decoration of the metal surface analogous to the SMSI behavior of reducible metal supports, which has been shown to suppress carbon deposition by breaking up large active site ensembles or altering the electron density of metal crystallites.[42][43] On the other hand, this could also be an effect similar to lanthanum oxide or ceria supports where dual metal and support sites separately activate CH_4 and CO_2, respectively, facilitating reaction at the metal/support interface.[44][45] Although further mechanistic studies would be required, this observation provides a possible direction for improving metal catalysts supported on stable and "inert" supports. This approach would not require control of the particle size but instead would employ overcoats of non-reducible oxides to obtain favorable reaction kinetics directly at the active site. The effect of carbon deposition on the rate of deactivation was not measured here, but we have shown for a very similar uncoated 2 wt% Ni/θ-Al_2O_3 catalyst that the contribution of carbon deposition to the rate of deactivation is negligible,[46] particularly in comparison to the rates of activity change shown here. However, we did not investigate the effects of carbon deposition on overcoated catalysts.

In summary, the exact nature of the effect of the overcoat on the DRM active site requires further investigation, although the present results clearly indicate the beneficial effects of an ALD overcoat for enhancing catalyst stability. Furthermore, "tuning" the Ni loading and pre-treatment conditions is a synthetic strategy to maximize the favorable effects of a thermally stable alumina overcoat whilst avoiding preferential $NiAl_2O_4$ formation and reduction under DRM conditions. Explicitly, the oxidation state of Ni during annealing of the material is likely critical to this strategy.

4. Conclusions

Application of an ALD alumina overcoat can significantly enhance the catalytic stability of a dispersed Ni catalyst on an industrially relevant oxide support for the harsh methane dry reforming reaction. We find that an uncoated catalyst deactivates principally by Ni sintering. Overcoating the catalyst lowers both the rate of Ni sintering and the rate of carbon deposition. Furthermore, it is shown that formation of $NiAl_2O_4$ is not a catalyst deactivation pathway. Instead, reduction of this phase to Ni/Al_2O_3 occurs under DRM conditions, slowly increasing catalytic activity. This slow reduction of Ni^{2+} in the $NiAl_2O_4$ lattice to the active Ni metal is likely the cause of the slow increase in activity for alumina supported Ni catalysts calcined at high temperatures and certain alumina overcoated Ni

catalysts. Further research will focus on elucidating the contributions of individual mechanisms towards the rates of activity change and carbon deposition, and methods of stabilizing overcoated Ni against slow deactivation at longer timescales.

Acknowledgements

This work was made possible by a NPRP exceptional grant award [NPRP-EP X-100-2-024] from the Qatar National Research Fund (a member of the Qatar Foundation). The statements made herein are solely the responsibility of the authors. The CleanCat Core facility acknowledges funding from the Department of Energy (DE-SC0001329) used for the purchase of the Altamira BenchCat 4000. This work made use of the Jerome B. Cohen X-Ray Diffraction Facility supported by the MRSEC program of the National Science Foundation (DMR-1720139) at the Materials Research Center of Northwestern University and the Soft and Hybrid Nanotechnology Experimental (SHyNE) Resource (NSF ECCS-1542205.) The authors would like to thank the groups of Prof. Kenneth R. Poeppelmeier for use of high temperature furnaces and Prof. Justin M. Notestein for use of UV-Vis-DRS equipment.

References

[1] M.M.B. Noureldin, N.O. Elbashir, M.M. El-Halwagi, Optimization and selection of reforming approaches for syngas generation from natural/shale gas, Ind. Eng. Chem. Res. 53 (2014) 1841–1855. doi:10.1021/ie402382w.

[2] J. Sehested, Four challenges for nickel steam-reforming catalysts, Catal. Today. 111 (2006) 103–110. doi:10.1016/j.cattod.2005.10.002.

[3] J.B. Claridge, M.L.H. Green, S.C. Tsang, A.P.E. York, A.T. Ashcroft, P.D. Battle, A study of carbon deposition on catalysts during the partial oxidation of methane to synthesis gas, Catal. Letters. 22 (1993) 299–305. doi:10.1007/BF00807237.

[4] C.H. Bartholomew, Mechanisms of catalyst deactivation, Appl. Catal. A Gen. 212 (2001) 17–60. doi:10.1016/S0926-860X(00)00843-7.

[5] J.R. Rostrup-Nielsen, J. Sehested, J.K. Nørskov, Hydrogen and synthesis gas by steam- and C02 reforming, Adv. Catal. 47 (2002) 65–139. doi:10.1016/S0360-0564(02)47006-X.

[6] Z. Bian, S. Das, M.H. Wai, P. Hongmanorom, S. Kawi, A Review on Bimetallic Nickel-Based Catalysts for CO2 Reforming of Methane, ChemPhysChem. 18 (2017) 3117–3134. doi:10.1002/cphc.201700529.

[7] B.J. Oneill, D.H.K. Jackson, J. Lee, C. Canlas, P.C. Stair, C.L. Marshall, J.W. Elam, T.F. Kuech, J.A. Dumesic, G.W. Huber, Catalyst design with atomic layer deposition, ACS Catal. 5 (2015) 1804–1825. doi:10.1021/cs501862h.

[8] C. Wang, H. Wang, Q. Yao, H. Yan, J. Li, J. Lu, Precisely Applying TiO2 Overcoat on Supported Au Catalysts Using Atomic Layer Deposition for Understanding the Reaction Mechanism and Improved Activity in CO Oxidation, J. Phys. Chem. C. 120 (2016) 478–486. doi:10.1021/acs.jpcc.5b11047.

[9] T.M. Onn, S. Zhang, L. Arroyo-Ramirez, Y.C. Chung, G.W. Graham, X. Pan, R.J. Gorte, Improved

Thermal Stability and Methane-Oxidation Activity of Pd/Al2O3 Catalysts by Atomic Layer Deposition of ZrO2, ACS Catal. 5 (2015) 5696–5701. doi:10.1021/acscatal.5b01348.

[10] Y. Hu, Y. Wang, Z.H. Lu, X. Chen, L. Xiong, Core-shell nanospheres Pt@SiO2for catalytic hydrogen production, Appl. Surf. Sci. 341 (2015) 185–189. doi:10.1016/j.apsusc.2015.02.094.

[11] J. Zhang, F. Li, Coke-resistant Ni@SiO2 catalyst for dry reforming of methane, Appl. Catal. B Environ. 176–177 (2015) 513–521. doi:10.1016/j.apcatb.2015.04.039.

[12] E. Baktash, P. Littlewood, R. Schomäcker, A. Thomas, P.C. Stair, Alumina coated nickel nanoparticles as a highly active catalyst for dry reforming of methane, Appl. Catal. B Environ. 179 (2015) 122–127. doi:10.1016/j.apcatb.2015.05.018.

[13] J. Lu, B. Fu, M.C. Kung, G. Xiao, J.W. Elam, H.H. Kung, P.C. Stair, Coking-and Sintering-Resistant Palladium Catalysts Achieved Through Atomic Layer Deposition, Science (80-.). 335 (2012) 1205–1208. doi:10.1126/science.1212906.

[14] T.D. Gould, A. Izar, A.W. Weimer, J.L. Falconer, J.W. Medlin, Stabilizing Ni Catalysts by Molecular Layer Deposition for Harsh, Dry Reforming Conditions, ACS Catal. 4 (2014) 2714–2717. doi:10.1021/cs500809w.

[15] R. -S Zhou, R.L. Snyder, Structures and transformation mechanisms of the η, γ and θ transition aluminas, Acta Crystallogr. Sect. B. 47 (1991) 617–630. doi:10.1107/S0108768191002719.

[16] J. Zieliński, Morphology of nickel/alumina catalysts, J. Catal. 76 (1982) 157–163. doi:10.1016/0021-9517(82)90245-7.

[17] J. Zieliński, Effect of water on the reduction of nickel/alumina catalysts Catalyst characterization by temperature-programmed reduction, J. Chem. Soc. Faraday Trans. 93 (1997) 3577–3580. doi:10.1039/a703392c.

[18] T. Margossian, K. Larmier, S.M. Kim, F. Krumeich, A. Fedorov, P. Chen, C.R. Müller, C. Copéret, Molecularly Tailored Nickel Precursor and Support Yield a Stable Methane Dry Reforming Catalyst with Superior Metal Utilization, J. Am. Chem. Soc. 139 (2017) 6919–6927. doi:10.1021/jacs.7b01625.

[19] A. Giehr, L. Maier, S.A. Schunk, O. Deutschmann, Thermodynamic considerations on the oxidation state of Co/γ-Al2O3 and Ni/γ-Al2O3 catalysts under dry and steam reforming conditions, ChemCatChem. (2017) 751–757. doi:10.1002/cctc.201701376.

[20] D. San José-Alonso, M.J. Illán-Gómez, M.C. Román-Martínez, Low metal content Co and Ni alumina supported catalysts for the CO2 reforming of methane, Int. J. Hydrogen Energy. 38 (2013) 2230–2239. doi:10.1016/j.ijhydene.2012.11.080.

[21] P. Kim, Y. Kim, H. Kim, I.K. Song, J. Yi, Synthesis and characterization of mesoporous alumina with nickel incorporated for use in the partial oxidation of methane into synthesis gas, Appl. Catal. A Gen. 272 (2004) 157–166. doi:10.1016/j.apcata.2004.05.055.

[22] A. Cimino, M. Lo Jacono, M. Schiavello, Structural, magnetic, and optical properties of nickel oxide supported on .eta.- and .gamma.-aluminas, J. Phys. Chem. 75 (1971) 1044–1050. doi:10.1021/j100678a005.

[23] I.S. Ahmed, H.A. Dessouki, A.A. Ali, Synthesis and characterization of NixMg1- xAl2O4 nano ceramic pigments via a combustion route, Polyhedron. 30 (2011) 584–591.

doi:10.1016/j.poly.2010.11.034.

[24] C.F. Song, M.K. Lü, F. Gu, S.W. Liu, S.F. Wang, D. Xu, D.R. Yuan, Effect of Al3+on the photoluminescence properties of Ni2+-doped sol-gel SiO2glass, Inorg. Chem. Commun. 6 (2003) 523–526. doi:10.1016/S1387-7003(03)00019-4.

[25] M. Jitianu, A. Jitianu, M. Zaharescu, D. Crisan, R. Marchidan, IR structural evidence of hydrotalcites derived oxidic forms, Vib. Spectrosc. 22 (2000) 75–86. doi:10.1016/S0924-2031(99)00067-3.

[26] E. Zannoni, E. Cavalli, A. Toncelli, M. Tonelli, M. Bettinelli, Optical spectroscopy of Ca3Sc2Ge3O12:Ni2+, J. Phys. Chem. Solids. 60 (1999) 449–455. doi:10.1016/S0022-3697(98)00314-X.

[27] B. Vos, E. Poels, A. Bliek, Impact of calcination conditions on the structure of alumina-supported nickel particles, J. Catal. 198 (2001) 77–88. doi:10.1006/jcat.2000.3082.

[28] W.J. Jang, J.O. Shim, H.M. Kim, S.Y. Yoo, H.S. Roh, A review on dry reforming of methane in aspect of catalytic properties, Catal. Today. (2018). doi:10.1016/j.cattod.2018.07.032.

[29] M.D. Groner, F.H. Fabreguette, J.W. Elam, S.M. George, Low-Temperature Al2O3 Atomic Layer Deposition, Chem. Mater. 16 (2004) 639–645. doi:10.1021/cm0304546.

[30] S. Karwal, T. Li, A. Yanguas-Gil, C.P. Canlas, Y. Lei, A.U. Mane, J.A. Libera, S. Seifert, R.E. Winans, J.W. Elam, Tailoring nanopore formation in atomic layer deposited ultrathin films, J. Vac. Sci. Technol. A Vacuum, Surfaces, Film. 36 (2018) 1–103. doi:10.1116/1.4986202.

[31] C. George, Rational Design of Catalysts by Atomic Layer Deposition, Northwestern University, Evanston, IL, 2016.

[32] J.A. Varela, O.J. Whittemore, E. Longo, Pore size evolution during sintering of ceramic oxides, Ceram. Int. 16 (1990) 177–189. doi:10.1016/0272-8842(90)90053-I.

[33] R. López-Fonseca, C. Jiménez-González, B. de Rivas, J.I. Gutiérrez-Ortiz, Partial oxidation of methane to syngas on bulk NiAl2O4 catalyst. Comparison with alumina supported nickel, platinum and rhodium catalysts, Appl. Catal. A Gen. 437–438 (2012) 53–62. doi:10.1016/j.apcata.2012.06.014.

[34] B. Phillips, J.J. Hutta, I. Warshaw, Phase Equilibria in the System NiO-Al2O3-SiO2, J. Am. Ceram. Soc. 46 (1963) 579–583. doi:10.1111/j.1151-2916.1963.tb14620.x.

[35] L. Smolakova, M. Kout, L. Capek, A. Rodriguez-gomez, V.M. Gonzalez-Delacruz, L. Hromadko, A. Caballero, Nickel catalyst with outstanding activity in the DRM reaction prepared by high temperature calcination treatment, Int. J. Hydrog. Energy. 41 (2016) 8459–8469. doi:10.1016/j.ijhydene.2016.03.161.

[36] L. Zhang, X. Wang, X. Shang, M. Tan, W. Ding, X. Lu, Carbon dioxide reforming of methane over mesoporous nickel, J. Energy Chem. 26 (2017) 93–100. doi:10.1016/j.jechem.2016.08.001.

[37] K.P. Trumble, M. Rühle, The thermodynamics of spinel interphase formation at diffusion-bonded Ni/Al2O3 interfaces, Acta Metall. Mater. 39 (1991) 1915–1924. doi:10.1016/0956-7151(91)90160-3.

[38] K.O. Christensen, D. Chen, R. Lødeng, a. Holmen, Effect of supports and Ni crystal size on

carbon formation and sintering during steam methane reforming, Appl. Catal. A Gen. 314 (2006) 9–22. doi:10.1016/j.apcata.2006.07.028.

[39] M. Cargnello, P. Fornasiero, R.J. Gorte, Opportunities for Tailoring Catalytic Properties Through Metal-Support Interactions, Catal. Letters. 142 (2012) 1043–1048. doi:10.1007/s10562-012-0883-4.

[40] L. Zhou, L. Li, N. Wei, J. Li, J.-M. Basset, Effect of $NiAl_2O_4$ Formation on Ni/Al_2O_3 Stability during Dry Reforming of Methane, ChemCatChem. 7 (2015) 2508–2516. doi:10.1002/cctc.201500379.

[41] A.Y. Stakheev, L.. Kustov, Effects of the support on the morphology and electronic properties of supported metal clusters: modern concepts and progress in 1990s, Appl. Catal. A Gen. 188 (1999) 3–35. doi:10.1016/S0926-860X(99)00232-X.

[42] F.H. Ribeiro, A.L. Bonivardi, C. Kim, G.A. Somorjai, Transformation of platinum into a stable, high-temperature, dehydrogenation-hydrogenation catalyst by ensemble size reduction with rhenium and sulfur, J. Catal. 150 (1994) 186–198. doi:10.1006/jcat.1994.1335.

[43] M.C.J. Bradford, M.A. Vannice, Catalytic reforming of methane with carbon dioxide over nickel catalysts I. Catalyst characterization and activity, Appl. Catal. A Gen. 142 (1996) 73–96. doi:10.1016/0926-860X(96)00065-8.

[44] N. Laosiripojana, W. Sutthisripok, S. Assabumrungrat, Synthesis gas production from dry reforming of methane over CeO2 doped Ni/Al2O3: Influence of the doping ceria on the resistance toward carbon formation, Chem. Eng. J. 112 (2005) 13–22. doi:10.1016/j.cej.2005.06.003.

[45] Z. Zhang, X.E. Verykios, Mechanistic aspects of carbon dioxide reforming of methane to synthesis gas over Ni catalysts, Catal. Letters. 38 (1996) 175–179. doi:10.1007/BF00806565.

[46] P. Littlewood, E. Weitz, T.J. Marks, P.C. Stair, Kinetic Isoconversion Loop Catalysis: A Reactor Operation Mode To Investigate Slow Catalyst Deactivation Processes, with Ni/Al_2O_3 for the Dry Reforming of Methane, Ind. Eng. Chem. Res. (2018) acs.iecr.8b04320. doi:10.1021/acs.iecr.8b04320.

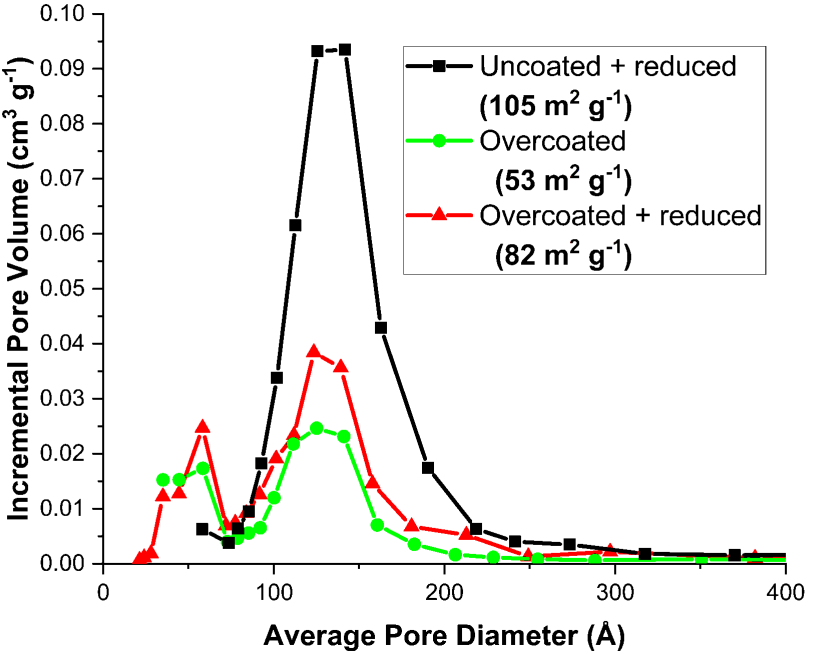
Incremental Pore Volume (cm^3 g^{-1})
0.10
0.09
0.08
0.07
0.06
0.05
0.04
0.03
0.02
0.01
0.00
0
100
200
300
400
Average Pore Diameter (Å)
Uncoated + reduced
(105 m^2 g^{-1})
Overcoated
(53 m^2 g^{-1})
Overcoated + reduced
(82 m^2 g^{-1})

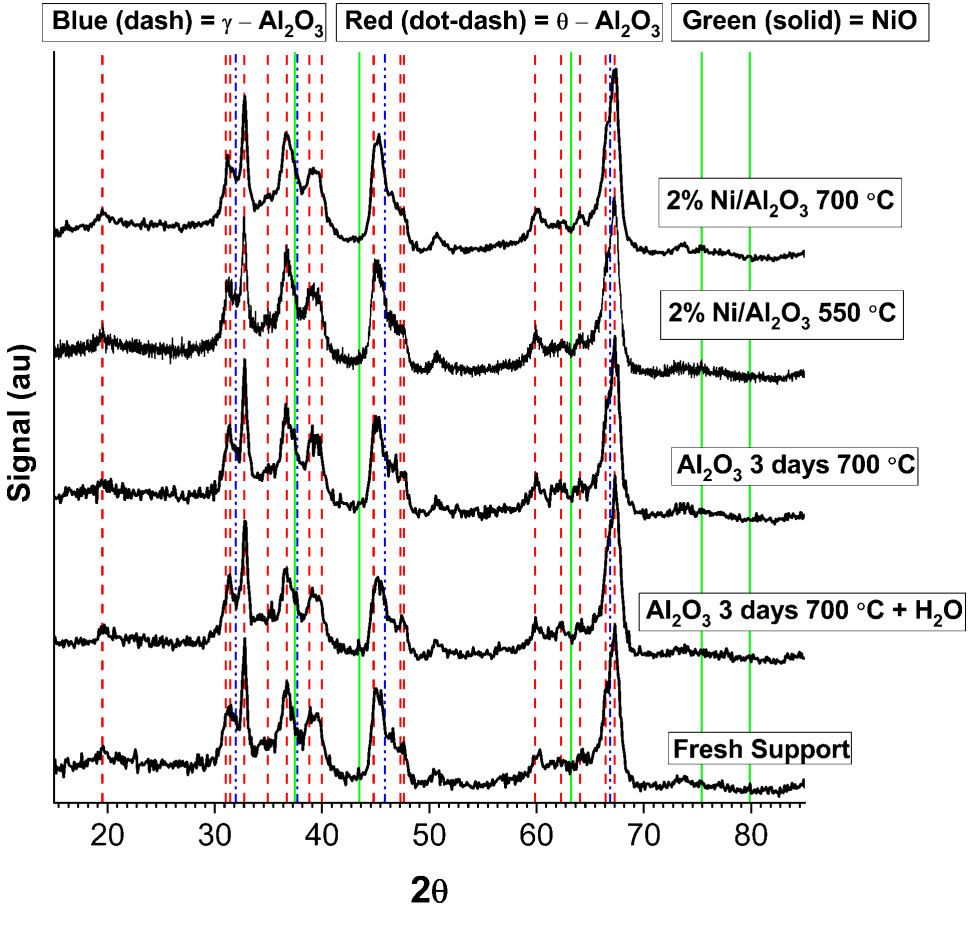
Blue (dash) = γ – Al2O3
Red (dot-dash) = θ – Al2O3
Green (solid) = NiO
2% Ni/Al2O3 700 °C
2% Ni/Al2O3 550 °C
Al2O3 3 days 700 °C
Al2O3 3 days 700 °C + H2O
Fresh Support
Signal (au)
20
30
40
50
60
70
80
2θ

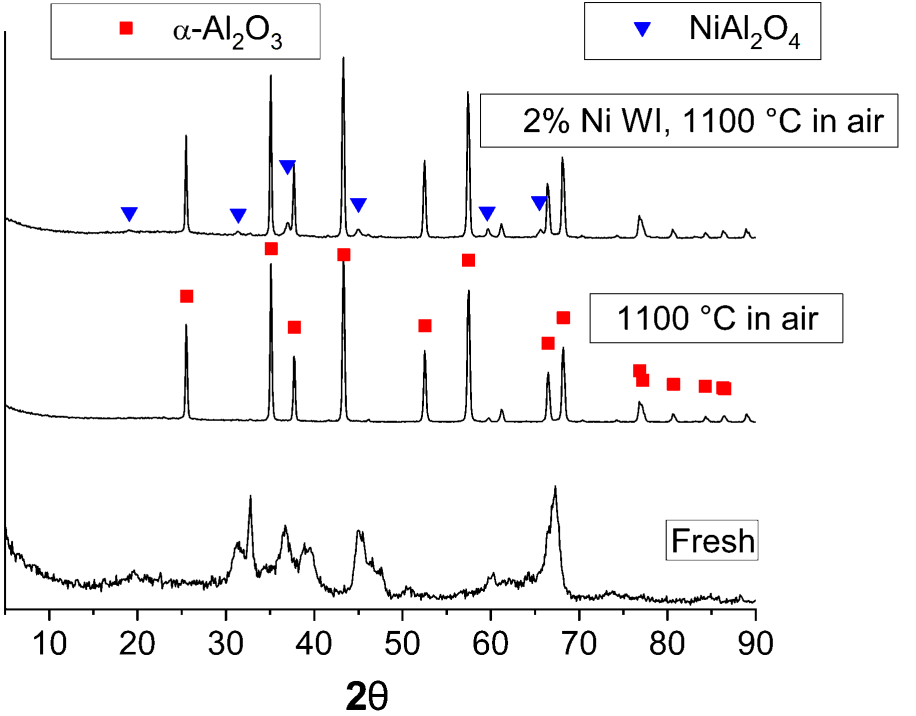
α-Al2O3
NiAl2O4
2% Ni WI, 1100 °C in air
1100 °C in air
Fresh
10
20
30
40
50
60
70
80
90
2θ

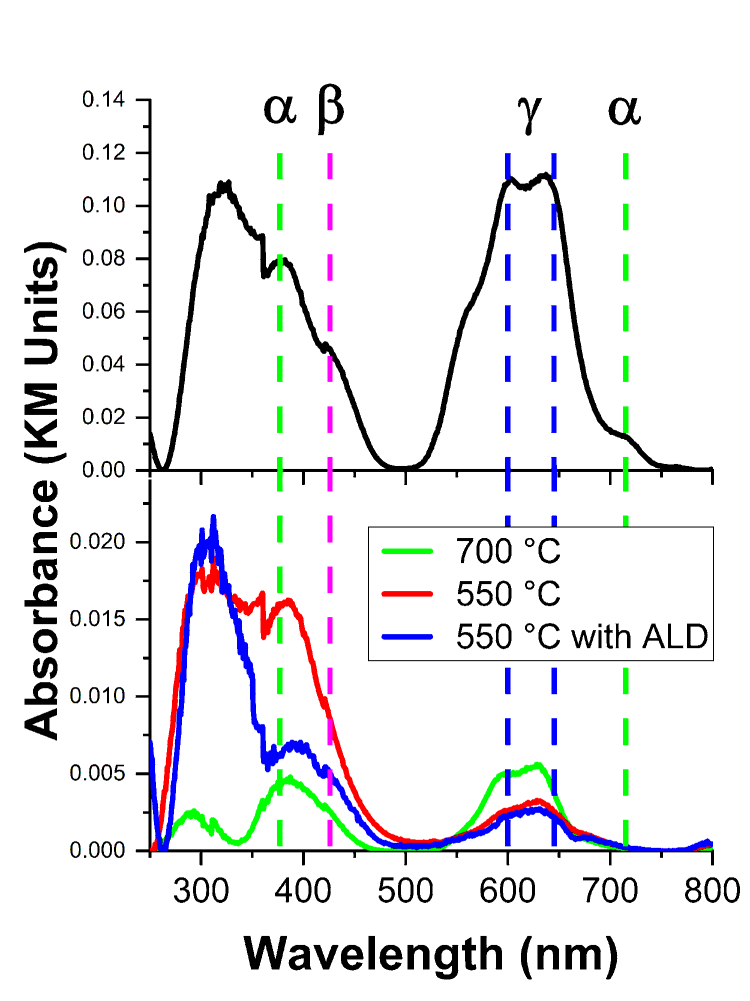
α
β
γ
α
0.14
0.12
0.10
0.08
0.06
0.04
0.02
0.00
0.020
0.015
0.010
0.005
0.000
700 °C
550 °C
550 °C with ALD
Absorbance (KM Units)
300
400
500
600
700
800
Wavelength (nm)

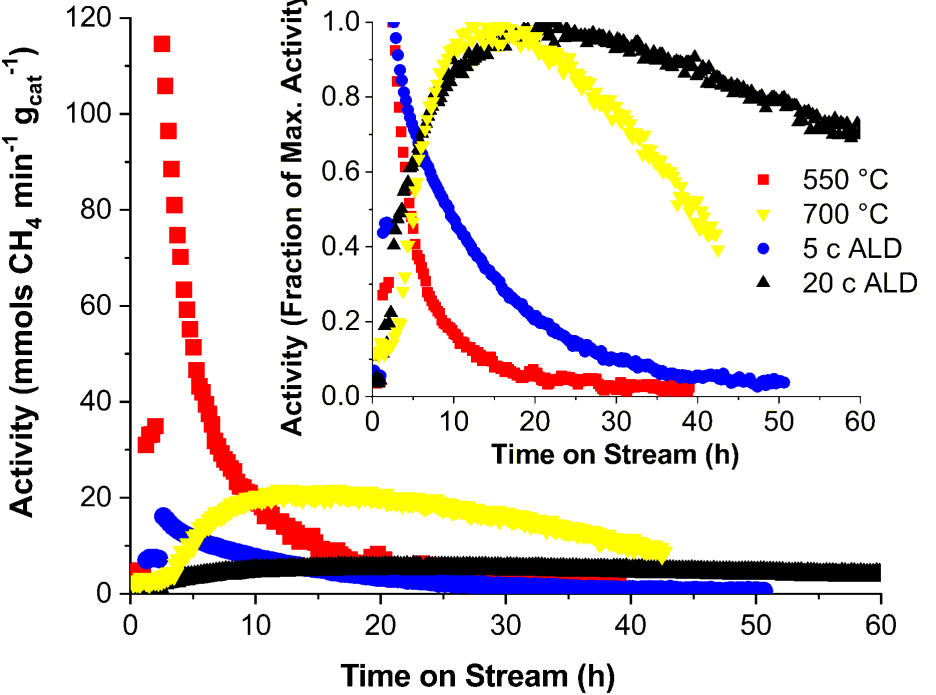
Activity (mmols CH_4 min^{-1} g_{cat}^{-1})
Time on Stream (h)
Activity (Fraction of Max. Activity)
Time on Stream (h)
550 °C
700 °C
5 c ALD
20 c ALD

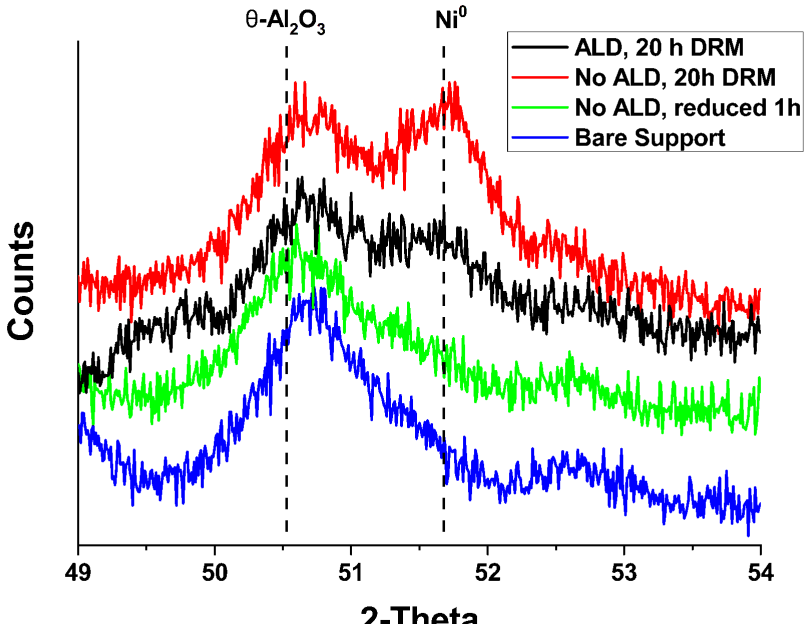
θ-Al2O3
Ni0
ALD, 20 h DRM
No ALD, 20h DRM
No ALD, reduced 1h
Bare Support
Counts
49
50
51
52
53
54
2-Theta

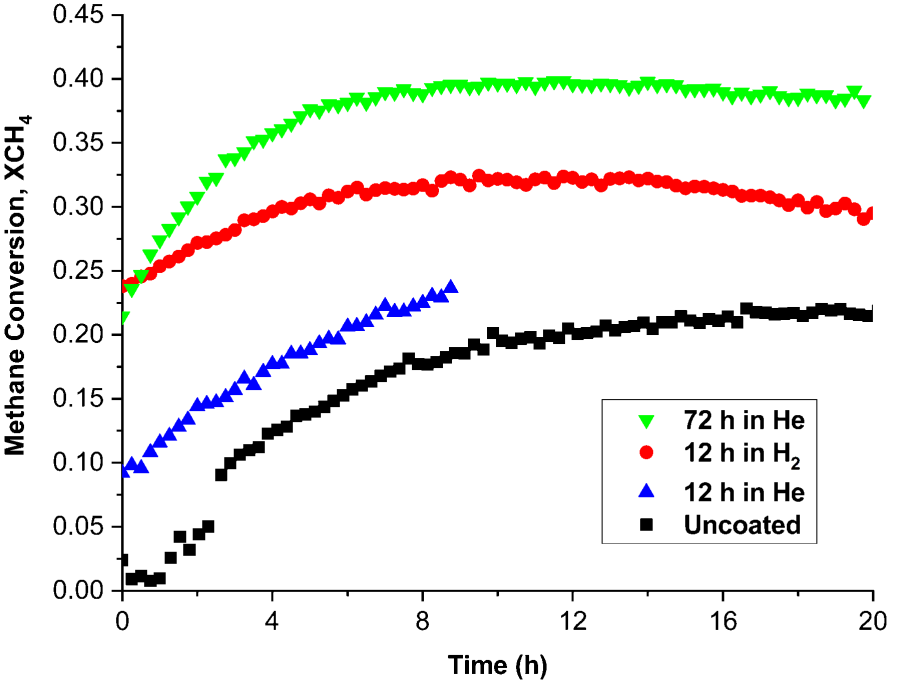
Methane Conversion, XCH_4
0.45
0.40
0.35
0.30
0.25
0.20
0.15
0.10
0.05
0.00
0
4
8
12
16
20
Time (h)
72 h in He
12 h in H_2
12 h in He
Uncoated

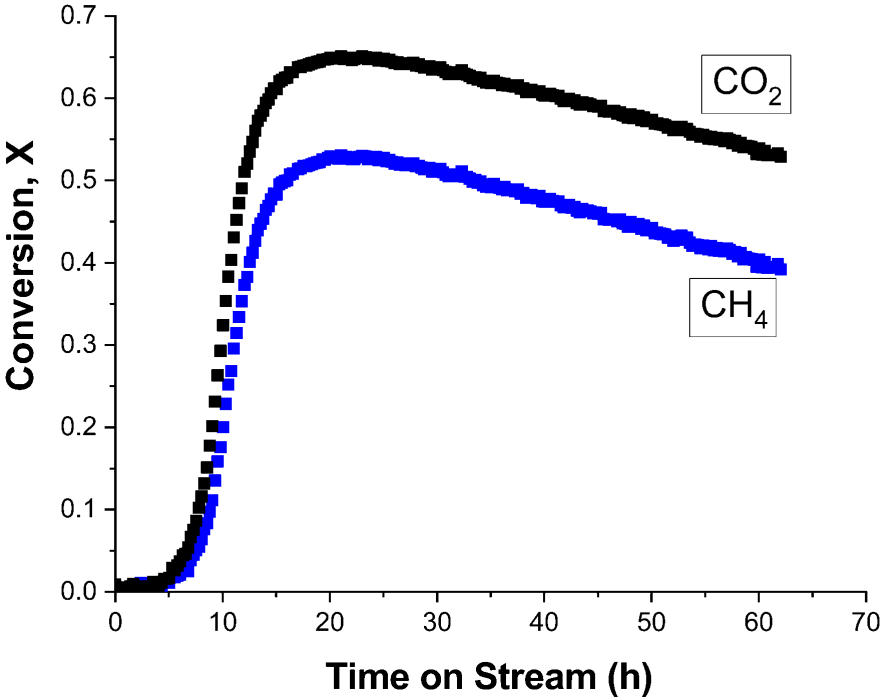
Conversion, X
Time on Stream (h)
CO2
CH4
0.0
0.1
0.2
0.3
0.4
0.5
0.6
0.7
0
10
20
30
40
50
60
70

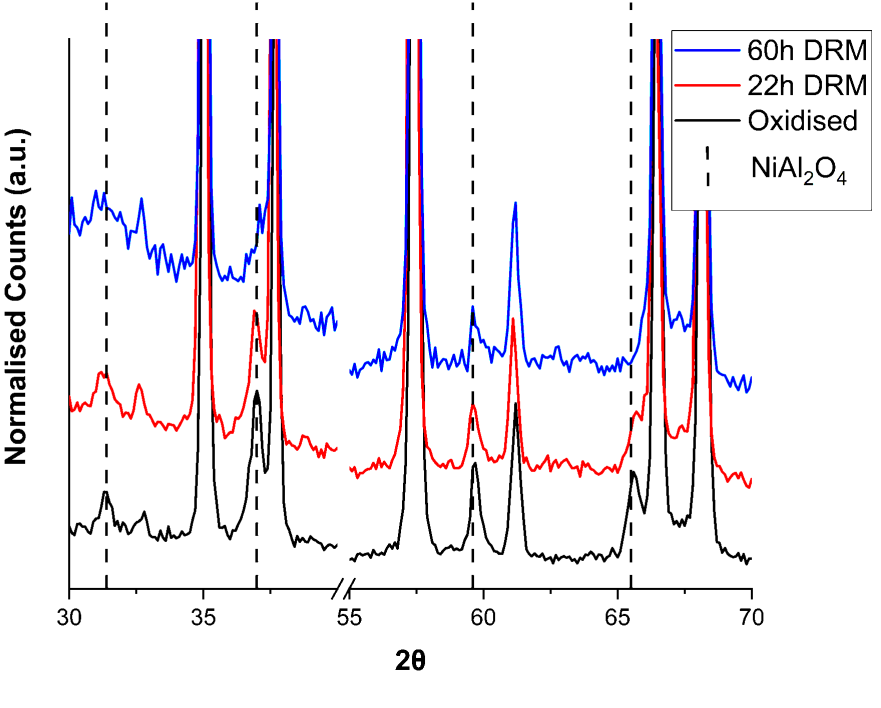
60h DRM
22h DRM
Oxidised
NiAl2O4
Normalised Counts (a.u.)
30
35
55
60
65
70
2θ

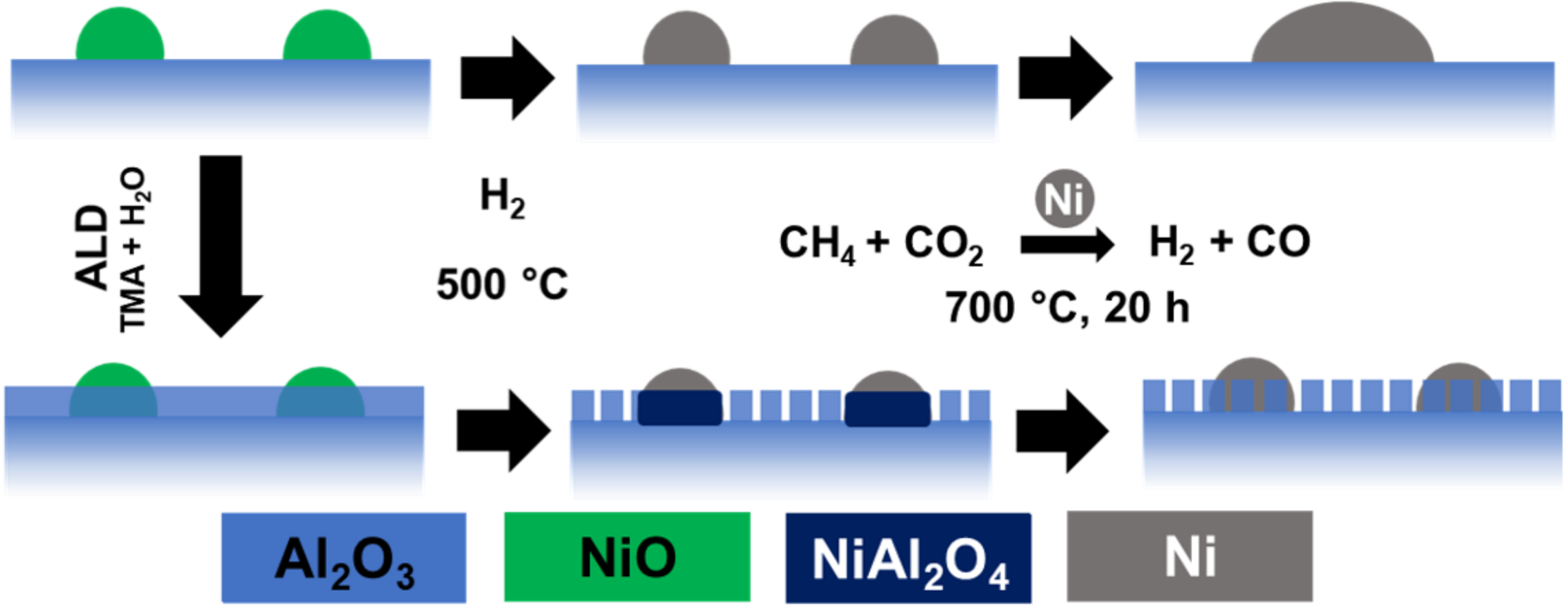
ALD
TMA + H2O
H2
500 °C
Ni
CH4 + CO2
H2 + CO
700 °C, 20 h
Al2O3
NiO
NiAl2O4
Ni